Grotthus-Type and Diffusive Proton Transfer in 7-Hydroxyquinoline•$(NH_3)_n$ Clusters

Markus Meuwly,*,† Andreas Bach,‡ and Samuel Leutwyler*

Contribution from the Departement für Chemie und Biochemie, Universität Bern, Freiestrasse 3, CH-3000 Bern 9, Switzerland

Received April 6, 2001

Abstract: Proton translocation along ammonia wires is investigated in 7-hydroxyquinoline•$(NH_3)_n$ clusters, both experimentally by laser spectroscopy and theoretically by Hartree−Fock and density functional (DFT) calculations. These clusters serve as realistic finite-size models for proton transfer along a chain of hydrogen-bonded solvent molecules. In the enol tautomer of 7-hydroxyquinoline (7-HQ), the OH group acts as a proton injection site into the $(NH_3)_n$ cluster. Proton translocation along a chain of three NH_3 molecules within the cluster can take place, followed by reprotonation of 7-HQ at the quinolinic N atom, forming the 7-ketoquinoline tautomer. Exoergic proton transfer from the OH group of 7-HQ to the closest NH_3 molecule within the cluster giving a zwitterion 7-HQ^-•$(NH_3)_6H^+$ (denoted PT-A) occurs at a threshold cluster size of $n = 6$ in the DFT calculations and at $n = 5$ or 6 experimentally. Three further locally stable zwitterion clusters denoted PT-B, PT-B′, and PT-C, the keto tautomer, and several transition structures along the proton translocation path were characterized theoretically. Grotthus-type proton-hopping mechanisms occur for three of the proton transfer steps, which have low barriers and are exoergic or weakly endoergic. The step with the highest barrier involves a complex proton transfer mechanism, involving structural reorganization and large-scale diffusive motions of the cluster.

Introduction

The transport properties of a solvated proton are of fundamental interest for acid−base chemistry,[1−4] enzymatic proton transfer,[5−8] and the possible relevance of proton wires and related concepts to biological systems.[9−17] Especially questions relating to the connection between solvent structure, solvent polarity, and proton transfer dynamics are of eminent importance.[18−25]

Historically, many different models have been proposed to rationalize the unusually high mobility of protons in water. The Grotthus mechanism[26] postulates a dynamical proton "shuttle" process in which molecules collectively exchange hydrogen and chemical bonds, resulting in a proton migration without requiring much translational motion of individual molecules. The net effect is the fast diffusion of the hydronium ion (H_3O^+) structure. A *precise* description of the mechanisms for proton transfer in bulk water is still difficult[27] despite the availability of modern computer simulations.[1,18−25] There is no single, simple mechanism that can grasp the complexity of proton transfer in protic solvents. The question how proton transfer occurs in ammonia clusters and along "ammonia wires" is at the heart of the present work.

Experimental investigations of proton transfer mechanisms are possible on clusters that are sufficiently large and complex to exhibit the characteristic features associated with proton transfer such as breaking and re-formation of both hydrogen and chemical bonds, proton solvation, and structural reorganization of the solvent. On the other hand, clusters are also small enough to allow accurate quantum chemical calculations to be performed for the electronic ground state. 7-hydroxyquinoline (7-HQ) has two potentially reactive groups that can serve as

† Current address: Laboratoire de Chimie Biophysique, Institut Le Bel, Université Louis Pasteur, 4, rue Blaise Pascal, 67000 Strasbourg, France.
‡ Current address: Department of Chemistry, University of Wisconsin, Madison, WI 53706.

(1) Warshel, A. *J. Phys. Chem.* **1982**, *86*, 2218.
(2) In *Proton Transfer in Hydrogen-Bonded Systems*; Bountis, T., Ed.; Plenum Press: New York, 1992; p 1922..
(3) Borgis, D.; Hynes, J. *Chem. Phys.* **1993**, *170*, 315.
(4) Staib, A.; Borgis, D.; Hynes, J. T. *J. Chem. Phys.* **1995**, *102*, 2487.
(5) Hwang, J.-K.; Warshel, A. *J. Am. Chem. Soc.* **1996**, *118*, 11745.
(6) Grochowski, P.; Lesyng, B.; Bala, P.; McCammon, J. A. *Int. J. Quantum Chem.* **1996**, *60*, 1143.
(7) Schmitt, U.; Voth, G. A. *J. Phys. Chem. B* **1998**, *102*, 5547.
(8) Agarwal, P. K.; Webb, S. P.; Hammes-Schiffer, S. *J. Am. Chem. Soc.* **2000,** *122*, 803.
(9) Nagle, J. F.; Morowitz, H. J. *Proc. Natl. Acad. Sci. U.S.A.* **1978**, *75*, 298.
(10) Warshel, A. *Photochem. Photobiol.* **1979**, *30*, 285.
(11) Nagle, J. F.; Tristram-Nagle, S. *J. Membr, Biol.* **1983**, *74*, 1.
(12) Hille, B. *Ionic Channels of Excitable Membranes*; Sinauer: Sunderland, MA, 1984.
(13) Warshel, A. *Methods Enzymol.* **1986**, *127*, 578.
(14) Pebay-Peroula, E.; Rummel, G.; Rosenbusch, J. P.; Landau, E. M. *Science* **1997**, *277*, 1676.
(15) Luecke, H.; Richter, H.-T.; Lanyi, J. K. *Science* **1998**, *280*, 1934.
(16) Luecke, H.; Schobert, B.; Richter, H.-T.; Cartailler, J.; Lanyi, J. K. *Science* **1999**, *286*, 255.
(17) Sham, Y. Y.; Muegge, I.; Warshel, A. *Proteins: Struct., Funct. Genet.* **1999**, *36*, 484.
(18) Aqvist, J.; Warshel, A. *Chem. Rev.* **1993**, *93*, 2529.
(19) Tuckerman, M.; Laasonen, K.; Sprik, M.; Parrinello, M. *J. Phys. Chem.* **1995**, *99*, 5749.
(20) Pomès, R.; Roux, B. *Biophys. J.* **1996**, *71*, 19.
(21) Tuckerman, M.; Marx, D.; Klein, M. L.; Parrinello, M. *Science* **1997**, *275*, 817.
(22) Vuilleumier, R.; Borgis, D. *Chem. Phys. Lett.* **1998**, *284*, 71.
(23) Vuilleumier, R.; Borgis, D. *J. Phys. Chem. B* **1998**, *102*, 4261.
(24) Mei, H. S.; Tuckerman, M. E.; Sagnella, D. E.; Klein, M. L. *J. Phys. Chem. B* **1998**, *102*, 10446.
(25) Marx, D.; Tuckerman, M. E.; Hutter, J.; Parrinello, M. *Nature* **1999**, *397*, 601.
(26) von Grotthus, C. J. D. *Ann. Chim.* **1806**, *58*, 54.
(27) Agmon, N. *Chem. Phys. Lett.* **1995**, *244*, 456.

10.1021/ja010893a CCC: $20.00
Published on Web 10/27/2001

either a proton donor or a proton acceptor.[28−31] In its enol form, the OH acts as the proton donor, and the nitrogen atom is the acceptor. In the 7-ketoquinoline (7-KQ) tautomer, the roles are reversed. It has been shown experimentally that 7-HQ·$(NH_3)_n$ clusters support proton transfer to the finite-size cluster for $n \geq 4$ in the S_1 excited and for $n \geq 6$ in the S_0 ground state, while for $n \leq 3$, no proton transfer is observed in either the S_0 or S_1 state.[31,32] Both the 7-HQ and 7-KQ tautomers can act as acid and/or base toward the ammonia cluster, in the S_1 or the S_0 state. Proton transfer can occur toward and along a network of ammonia molecules, whereby the cluster acts as a proton acceptor, or a proton "wire" system.[32]

However, the analysis of the cluster size dependent spectroscopic features is not straightforward and needs assistance by theory. Recently, we calculated the topologies, structures, and binding energies of a large set of 7-HQ·$(NH_3)_n$ cluster isomers at the SCF level.[33] Here, we describe new experimental results and extensive ab initio theoretical studies, employing also density functional theory (DFT) methods with larger basis sets to elucidate the mechanisms of the cluster ground-state proton transfer and tautomerization processes.

We address the following questions: What are the potential energy profiles of the proton transfer paths starting from both the enol and keto tautomers of 7-HQ? Are there locally or even globally stable structures corresponding to ion-pair (zwitterion) 7-HQ·$(NH_3)_n$ clusters? On the basis of these results, is exoergic proton transfer possible in the electronic ground state of 7-HQ·$(NH_3)_n$ clusters? If yes, what is the threshold cluster size *n*? What are the structures and energies of other identifiable zwitterionic intermediates along the PT path? Finally, do the proton transfer paths reflect Grotthus-type/proton-hopping mechanisms or more complex behavior?

Experimental and Computational Procedures

Experimental Methods. The experimental setup was described in refs 23 and 24. Briefly, 7-HQ·$(NH_3)_n$ clusters were synthesized and cooled in a 20 Hz pulsed supersonic beam of Ne mixed with 1% NH_3. Two-color resonant two-photon ionization (2C-R2PI) spectra were measured by crossing the skimmed beam with overlapping excitation and ionization laser beams inside the source of a linear time-of-flight mass spectrometer. The $S_1 \leftarrow S_0$ excitation was induced with the frequency-doubled UV output or the fundamental of a pulsed dye laser pumped by either the 355 or 532 nm output of a Nd:YAG laser. In the 389−412 nm range, sum-frequency mixing (SFM) in BBO of the fundamental of a pulsed dye laser and the residual 1.06 μm Nd:YAG output was used. For the ionization step, a second UV dye laser was employed, which was fully spatially and temporally overlapped with the excitation pulse. Typical dye laser pulse energies ranged from 0.1 to 1.0 mJ/pulse for excitation and 1 mJ/pulse for ionization. The spectra are corrected for laser power fluctuations.

For $n = 4$, the ionization wavelength was set to 292.5 nm, closely above the onset of the two-color photoion signal threshold at ∼61 700 cm^{-1}. For the clusters with $n \geq 5$, the ionization wavelength was lowered to 287.5 nm (∼58 800 cm^{-1}). As is the case with all 2C-R2PI experiments that start from a neutral cluster species and detect the cluster ion, cluster dissociation may occur between the excitation and the detection step or following ionization. However, based on the lack of observable cluster dissociation for the smaller 7-HQ·$(NH_3)_{1-4}$ clusters, we do not expect loss of more than one NH_3 molecule in the 2C-R2PI process.

Ab Initio Molecular Orbital Calculations. The ab initio calculations on 7-HQ·$(NH_3)_n$ were carried out at the Hartree−Fock level using the 6-31G(d,p) basis set and with the B3LYP density functional with the 6-311++G(d,p) basis set, using Gaussian98.[34] Structural optimizations were converged until the change in relative energy was $< 5 \times 10^{-7} E_h$, maximum forces and displacements were converged until they were $< 5 \times 10^{-4} E_h/a_0$ and $< 2 \times 10^{-3} a_0$, respectively. Once the optimization was close to the convergence criteria, only minor changes within the solvent shell were observed.

"Frozen" scans of the proton transfer energy profile were initiated from the respective enol or keto tautomer minimum-energy cluster structures, by constraining all coordinates except for the O−H (N−H) distance for enol (keto) 7-HQ. In the "relaxed" potential energy scans, the O−H or N−H coordinate was increased stepwise by 0.1 Å increments; all other coordinates were fully optimized at each successive step. No correction for basis set superposition error (BSSE) was applied, since we are not interested in the cluster binding or dissociation energies in this work.

We use the same nomenclature for the cluster topology as in ref 33: the first number denotes the ammonia cluster size *n*. We then distinguish hydrogen-bonded substructures called chains (*ch*), which link the O and N atom of the 7-hydroxyquinoline framework, and cycles (*cy*), which start from and reconnect to the OH group, the latter acting as both a H-bond donor and acceptor. Both chains and cycles can be bifurcated (symbolized by a preceding *b*). The number of ammonia molecules contained in the substructure is given after the substructure label. As an example, *cy*2 is a two-membered cycle. Thus, a complete description of a structure is (*n ch*k *cy*l). PT-*J*, J = A, B, C is used to designate zwitterionic (ion-pair) clusters resulting from successive proton transfer steps along an ammonia chain; i.e., PT-A refers to an ion pair formed by PT from the OH of 7-HQ to the nearest ammonia molecule.

Experimental Results and Discussion

2C-R2PI spectra of 7-HQ·$(NH_3)_n$ for clusters with $n = 3-6$ and 10 are shown in Figure 1. The spectra up to and including $n = 3$ show discrete and narrow bands with widths of 1−2 cm^{-1} given by the rotational band contours. The 2C-R2PI and the corresponding dispersed fluorescence spectra have been analyzed, and it has been clearly established that in the $n \leq 3$ clusters the 7-hydroxyquinoline is present as the *enol* tautomer in both the S_0 and S_1 states.[31,32]

For 7-HQ·$(NH_3)_4$, individual vibronic bands due to intermolecular vibrations can be observed in the 2C-R2PI spectrum from the electronic origin up to ∼400 cm^{-1} above. However, the vibronic bands now exhibit widths of 25−40 cm^{-1}, much broader than those observed for the $n \leq 3$ clusters. These bands are superimposed on a continuous background, whose intensity increases rapidly at ∼450 cm^{-1} above the origin. Additional inhomogeneous broadening due to multiple 7-HQ·$(NH_3)_4$ isomers cannot be excluded at this point.

For cluster sizes $n \geq 5$, the 2C-R2PI spectra change profoundly: the widths of the main absorption feature increase to 500−1000 cm^{-1}, and the band maximum is shifted to 28 000

(28) Bach, A.; Leutwyler, S. *Chem. Phys. Lett.* **1999**, *299*, 381.
(29) Bach, A.; Coussan, S.; Müller, A.; Leutwyler, S. *J. Chem. Phys.* **2000**, *112*, 1192.
(30) Bach, A.; Coussan, S.; Müller, A.; Leutwyler, S. *J. Chem. Phys.* **2000**, *113*, 9032.
(31) Coussan, S.; Bach, A.; Leutwyler, S. *J. Phys. Chem. A* **2000**, *104*, 9864−9873.
(32) Bach, A.; Leutwyler, S. *J. Chem. Phys.* **2000**, *112*, 560−565.
(33) Coussan, S.; Meuwly, M.; Leutwyler, S. *J. Chem. Phys.* **2001**, *114*, 3524 .
(34) Frisch, M. J.; Trucks, G. W.; Schlegel, H. B.; Scuseria, G. E.; Robb, M. A.; Cheeseman, J. R.; Zakrzewski, V. G.; Montgomery, J. A.; Jr., Stratmann, R. E.; Burant, J. C.; Dapprich, S.; Millam, J. M.; Daniels, A. D.; Kudin, K. N.; Strain, M. C.; Farkas, O.; Tomasi, J.; Barone, V.; Cossi, M.; Cammi, R.; Mennucci, B.; Pomelli, C.; Adamo, C.; Clifford, S.; Ochterski, J.; Petersson, G. A.; Ayala, P. Y.; Cui, Q.; Morokuma, K.; Malick, D. K.; Rabuck, A. D.; Raghavachari, K.; Foresman, J. B.; Cioslowski, J.; Ortiz, J. V.; Stefanov, B. B.; Liu, G.; Liashenko, A.; Piskorz, P.; Komaromi, I.; Gomperts, R.; Martin, R. L.; Fox, D. J.; Keith, T.; Al-Laham, M. A.; Peng, C. Y.; Nanayakkara, A.; Gonzalez, C.; Challacombe, M.; Gill, P. M. W.; Johnson, B.; Chen, W.; Wong, M. W.; Andres, J. L.; Gonzalez, C.; Head-Gordon, M.; Replogle, E. S.; Pople, J. A. Gaussian98, Revision A.2; Gaussian, Inc., Pittsburgh, PA, 1998.

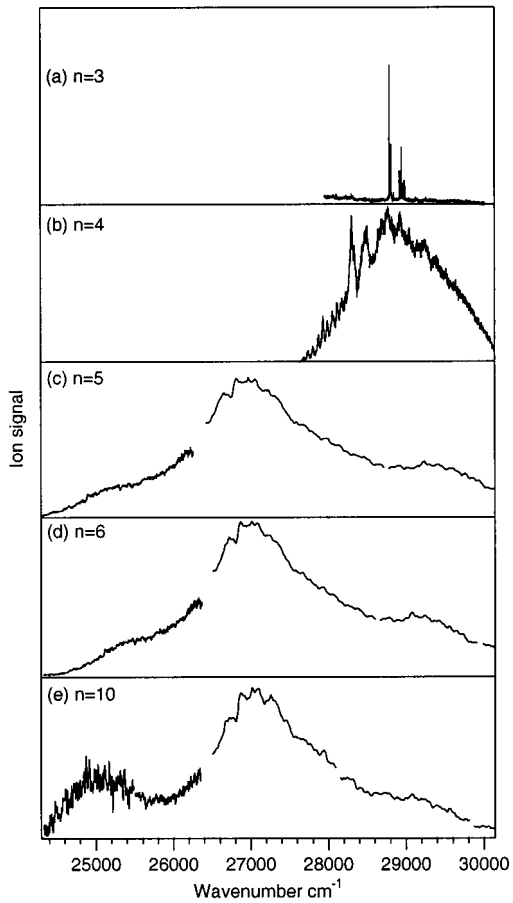

Figure 1. Two-color resonant two-photon ionization spectra for the 7-hydroxyquinoline·$(NH_3)_n$ clusters with $n = 3-6$ and $n = 10$.

cm^{-1}, almost 2000 cm^{-1} to the red of the electronic origin of the $n = 4$ cluster. For $n \geq 6$, an additional broad band appears, shifted to 26 000 cm^{-1}, a further 2000 cm^{-1} to the red. The intensity of this band is weaker than that of the 28 000 cm^{-1} band, but it increases with increasing cluster size *n*. The absolute signal intensities for the $n = 6$ and 10 spectra are much smaller than those for smaller *n*. The broad bands are reproducible, whereas the finer details are not.

The gradual loss of well-resolved vibrational patterns and the appearance of broad bands arising at longer wavelengths as the number of solvent molecules around the chromophore increases can be rationalized on the basis of previous experiments: bulk solution spectroscopic studies of 7-HQ in water and alcohols show that the enol species absorbs at $\lambda_{max} = 330-340$ nm (31 250 cm^{-1}), the 7-HQ^- anion at 370−375 nm (26 070−27 000 cm^{-1}) and the keto tautomer of 7-HQ at $\lambda_{max} \sim 400-420$ nm (23 800−25 000 cm^{-1}).[35−38] With increasing basicity of the solvent, the absorption wavelengths for the enol and keto tautomers shift slightly to the red and blue, respectively. In methanol, the energy difference between the two absorption maxima is 7450 cm^{-1}, decreasing to 5300 cm^{-1} for water.

Starting at the cluster size $n = 5$ (possibly $n = 6$, because of dissociative loss of one NH_3, see above) a strong absorption band appears at 370 nm (27 000 cm^{-1}). It remains the most intense feature in the 2C-R2PI spectra up to $n = 10$. We believe that it corresponds to the 370−375 nm absorption band in bulk solutions of 7-HQ at high pH, attributed to the ground-state 7-HQ^- anion.[35−38] Hence, we assign this band to formation of the ion-pair or zwitterion 7-HQ^-·$H^+(NH_3)_n$ clusters in the electronic ground state. For $n \geq 6$ clusters a further absorption feature appears at 385 nm (26 000 cm^{-1}), whose intensity shifts to the red and increases with increasing cluster size, relative to the band at 370 nm. Reasoning again by analogy with the bulk solution results, this 385−400 nm absorption band is tentatively assigned to absorption from the ground-state 7-ketoquinoline clusters. These assignments imply that for ammonia cluster sizes $n < 5$ only, the enol tautomer is stable and there are no local minima corresponding to either zwitterion or keto structures. For $n = 5$ or 6, proton injection into the cluster occurs and the 7-HQ^- anion becomes the globally stable species.

To assist the interpretation of these findings, extensive ab initio calculations have been carried out, which are described in the following. The results give a very detailed step-by-step picture of proton transfer in these ammonia−wire clusters, and their relation to the experimental observations is discussed.

Theoretical Results

A. Model Systems: The Proton-Bridged Dimers $NH_3\cdots H^+\cdots H_2O$ and $H_3N\cdots H^+\cdots NH_3$. In the most localized view, the PT reactions in 7-HQ·$(NH_3)_n$ proceed first by translocation of a proton from the OH group of 7-HQ to the proximal hydrogen-bonded NH_3 and then by further transfers between NH_3 molecules along the cluster network. To gain a deeper understanding for the dependence of the calculated proton transfer potentials and barrier heights on the level of theory employed, two smaller model systems were investigated, the proton-bound dimers $H_2O\cdots H^+\cdots NH_3$ and $H_3N\cdots H^+\cdots NH_3$.[39−42] The former is taken to model the proton transfer from the OH group of 7-HQ to the $(NH_3)_n$ cluster, the latter to represent the subsequent proton transfer steps within the ammonia cluster.

Calculations were performed at the same levels of theory as for 7-HQ·$(NH_3)_n$. For both systems, additional MP2 calculations were performed with the large aug-cc-VTZ (aVTZ) basis set.[43] In the calculation of the energy profiles for the proton transfer profiles of $H_3N\cdots H^+\cdots NH_3$ and $H_3N\cdots H^+\cdots OH_2$, the distance of the transferring proton with respect to the (or one) N atom was fixed, and all other coordinates were optimized.

Figure 2 shows cuts through the potential energy surface of $H_3N\cdots H^+\cdots NH_3$, where the $N-H^+$ bond length was used as the driving coordinate. All other degrees of freedom were optimized, and no linearity for the $N\cdots H^+\cdots N$ bond was assumed. At the SCF/6-31G(d,p) level, the barrier to proton transfer is $E_{TS} = 3.2$ kcal/mol; at the MP2/aVTZ level it decreases to 0.8 kcal/mol, and further to 0.4 kcal/mol at the B3LYP/6-311++(d,p) level. The minimum energy and transition-state geometries and the respective energies for the three methods are gathered in Table 1. The MP2/aVTZ barrier height can be compared to $E_{TS} = 0.9$ kcal/mol calculated by Jaroszewski et al. at the MP2/6-31G* level.[39] The optimized geometries of $H_3N\cdots H^+\cdots NH_3$ are in good agreement with previous studies using the MP2 method with smaller basis sets.[39,40]

Although the $H_2O\cdots H^+\cdots NH_3$ species is chemically not equivalent to the situation in the cluster and does not exhibit a

(35) Mason, S. F.; Philip, J.; Smith, B. E. *J. Chem. Soc. A* **1968**, 3051.
(36) Thistlethwaite, P. J.; Corkill, P. J. *Chem. Phys. Lett.* **1982**, *85*, 317.
(37) Thistlethwaite, P. J. *Chem. Phys. Lett.* **1983**, *96*, 509.
(38) Tokumura, K.; Itoh, M. *J. Phys. Chem.* **1984**, *88*, 3921.
(39) Jaroszewski, L.; Leysing, B.; Tanner, J. T.; McCammon, J. A. *Chem. Phys. Lett.* **1990**, *175*, 282.
(40) Ikuta, S. *J. Chem. Phys.* **1987**, *87*, 1900.
(41) Bala, P.; Grochowski, P.; Lesyng, B.; McCammon, J. A. *J. Phys. Chem.* **1996**, *100*, 2535.
(42) Sadukhan, S.; Munoz, D.; Adamo, C.; Scuseria, G. E. *Chem. Phys. Lett.* **1999**, *306*, 83.
(43) Woon, D. E.; Dunning, T. H. Jr. *J. Chem. Phys.* **1993**, *98*, 1358.

Table 1. Comparison of Optimized Minimum Energy and Transition State Structures and Energies of $H_3N\cdots H^+\cdots NH_3$ and $NH_3\cdots H^+\cdots OH_2$ at Different Levels of ab initio Theory[a]

	SCF/6−31G(d,p)	B3LYP/6−311++G(d,p)	MP2/aVTZ	MP2/6−31G [a]
$H_3N\cdots H^+\cdots NH_3$				
R(N···N)	2.791	2.696	2.695	2.731
r(N−H)	1.064	1.141	1.112	1.115
E_{tot}/E_h	−112.782 84	−113.548 06	−113.3348 3	−113.110 83
E_{TS}	3.16	0.33	0.78	0.87
$NH_3\cdots H^+\cdots OH_2$				
R(N···O)	2.777	2.701	2.691	2.710
r(N−H)	1.024	1.064	1.051	1.064
E_{tot}/E_h	−132.603 46	−133.413 96	−133.192 00	−132.941 61
E_{TS}[2]	52.7	40.6	46.2	42.6

[a] All distances in Å, energies in kcal/mol unless otherwise stated. [b] Reference 39. [c] At R(N···O) = 3.25 Å.

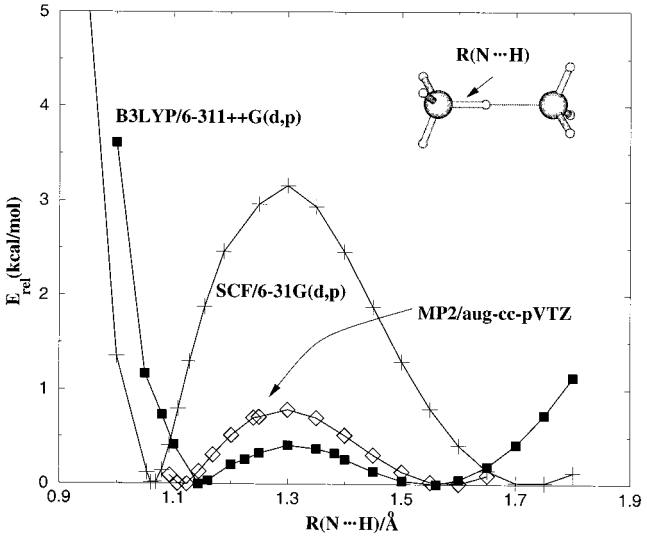

Figure 2. Potential energy curves for proton translocation in $H_3N\cdots H^+\cdots NH_3$, calculated at the SCF/6-31G(d,p), MP2/aug-cc-pVTZ, and B3LYP/6-311++G(d,p) levels of theory. Full geometry optimization was performed for each N···H distance. Total energies are plotted with respect to the minimum energies at the respective level.

local minimum for the $H_2OH^+\cdots NH_3$ form, it serves to calibrate the theoretical methods for the initial proton transfer step in 7-HQ·$(NH_3)_n$. For the mixed $(NH_3\cdots H\cdots H_2O)^+$ dimer, only a single minimum was found in the range of hydrogen bond distances R(N···O) = 2.7−2.9 Å, which corresponds to the $H_2O\cdots NH_4^+$ configuration. Following the approach taken in the MP2/6-31G* calculations of Jaroszewski et al.,[39] the N···O distance was stretched to 3.25 Å, which leads to an asymmetric double well potential. The calculated N−H → O barrier heights at this distance are E_{TS} = 40.6 [B3LYP/6-311++(d,p)], 46.2 [MP2/aVTZ], and 52.7 kcal/mol at the SCF/6-31G(d,p) level; see also Table 1.

Taking MP2/aVTZ as the reference calculation, the results on both systems indicate that proton transfer barriers calculated at the SCF/6-31G(d,p) level are too high by 3−6 kcal/mol. Hence, the SCF proton transfer barriers for 7-HQ·$(NH_3)_n$ clusters given below should be considered as upper limits. The B3LYP/6-311++G(d,p) method tends to underestimate the height of proton transfer barriers, but for $H_3N\cdots H^+\cdots NH_3$, the absolute difference is <0.5 kcal/mol and the shape of the B3LYP proton transfer potential is very similar to the MP2 calculations. Also, the computational demand for B3LYP is about 2 orders of magnitude smaller than for MP2/aVTZ. MP2/aVTZ calculations would not possible on the much larger 7-HQ·$(NH_3)_n$ clusters.

B. 7-Hydroxyquinoline: Proton Transfer from the OH Group. Experimentally, the enol tautomer is found to be the stable form for 7-HQ·$(NH_3)_n$ clusters with $n \leq 4$.[29] Consequently, we first investigated the proton translocation from the OH group of 7-HQ to the closest NH_3 molecule in the cluster, which gives the 7-HQ anion bound to a protonated ammonia cluster, 7-$HQ^-\cdot NH_4^+(NH_3)_{n-1}$, denoted PT-A.

Calculations at the SCF Level. Figure 3a displays the variation of the total energy along the O−H···N proton translocation coordinate at the SCF/6-31G(d,p) level, using "frozen" cluster geometries, for cluster sizes n = 2−5 and for two different isomers of n = 6, (6 bch3 cy3) and (6 ch3 cy4 cy3). In all cases, the lowest energy structure (for n = 6, the two lowest energy structures) so far identified has been used. We point out that experiments have not yet provided structural assignments for n = 4−6, and the starting structures employed here should be viewed as representative for the experimental cluster structures. The energy is plotted relative to the minimum energy of the respective enol tautomer of each cluster. Distinct local minima corresponding to proton transferred configurations $O\cdots NH_4^+(NH_3)_{n-1}$ were found for all clusters studied. The PT reaction is always predicted to be endoergic, with reaction energies ranging from $\Delta_r E$ = +34.4 kcal/mol for n = 2 to $\Delta_r E$ = + 20.0 kcal/mol for n = 5 (5 ch3 cy3) and $\Delta_r E$ = +14 kcal/mol for n = 6 (6 bch3 cy3). Interestingly, the (6 ch3 cy4 cy3) isomer of n = 6 is predicted to have *larger* endoergicity than the n = 5 cluster. The barriers for reverse PT are around 3 kcal/mol.

Figure 3b shows the results of full structural optimizations for the PT-A clusters, starting from the respective frozen-cluster PT-A local minima in Figure 3a. These did *not* lead to locally stable PT-A forms for *any* cluster with $n \leq 5$; i.e., the optimization invariably involved proton back transfer to 7-HQ. Of the two n = 6 isomers investigated, the bifurcated isomer (6 bch3 cy3) allows stabilization of the proton transferred form PT-A, whereas (6 ch3 cy4 cy3) does not. In the former isomer, the hydrogen bond coordination of the acceptor N_AH_3, is 4-fold, whereas in the latter, N_AH_3 is only 3-fold H-bond coordinated. At the SCF level, the Mulliken atomic charge on the (N_A) atom of (6 bch3 cy3) is −0.95*e*, more negative by 0.05*e* than for (6 ch3 cy4 cy3). This makes the N_AH_3 molecule in (6 bch3 cy3) a better proton acceptor.

Allowing structural relaxation of (6 bch3 cy3) decreases the endoergicity of the PT reaction from $\Delta_r E$ = +14.0 kcal/mol to only +4.3 kcal/mol (see Figure 3b) and the forward PT barrier from E_{TS} = +17.1 kcal/mol to only +5.7 kcal/mol. The curvature of the $O^-\cdots H-N$ potential also decreases considerably.

Figure 3c shows that the intermolecular $O\cdots N_A$ distance couples strongly to the proton transfer motion, shrinking from 2.80 Å in the enol form to 2.47 Å at the transition state and

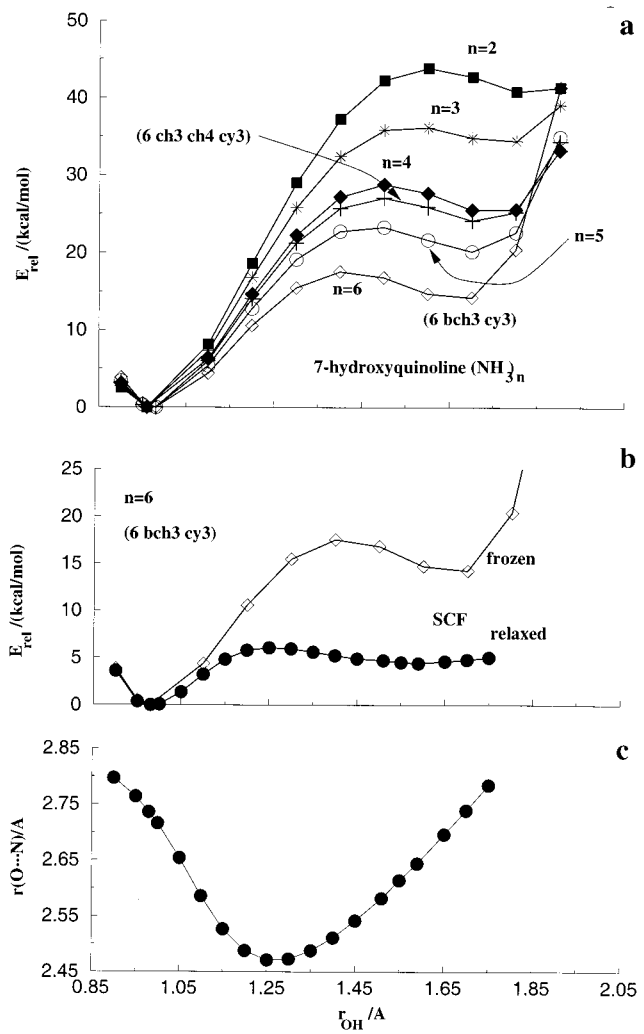

Figure 3. (a) SCF/6-31G(d,p) proton transfer potential energy curves along the O−H···N proton translocation coordinate in enol 7-HQ·$(NH_3)_n$, $n = 2-6$ clusters. Total energies are plotted with respect to the minimum energies of the respective cluster sizes. Cluster geometries were frozen at their respective enol minimum energy configurations; i.e., the O···N distances are different in every case. (b) SCF/6-31G-(d,p) proton transfer potential energy curves for the frozen and fully relaxed (6 bch3 cy3) clusters. (c) Change of the O···N distance as a function of the O···H separation for the (6 bch3 cy3) cluster in (b).

then expanding to 2.65 Å at the PT-A minimum. In parallel, the Mulliken atomic charges on the O, N_A, and H atom adjust in order to make the H-atom transfer energetically favorable. From enol → PT-A, the O atom becomes 15% more negative (−0.73*e* to −0.85*e*) and the N_A atom 15% less negative (−0.94*e* to −0.79*e*). The H atom has about the same charge in either configuration (0.44*e*) but becomes ∼20% more positive in the vicinity of the transition state (0.53*e*). The intramolecular structure parameter most influenced by the proton motion is the C−O bond lengths, which decreases by 5%.

Calculations at the B3LYP Level. The effects of electron correlation on the enol → PT-A proton transfer were then investigated using the B3LYP method. Full structural optimizations for (6 bch3 cy3) were carried out for the enol tautomer, in the vicinity of the PT transition state of the SCF/6-31G(d,p) calculation and for the PT-A zwitterion. A "frozen"-cluster geometry scan leads to a much shallower interaction potential than the SCF calculations, as shown in Figure 4. The barrier for formation of PT-A is $E_{TS} = 1.5$ kcal/mol, about 10 times smaller than the SCF/6-31G(d,p) value.

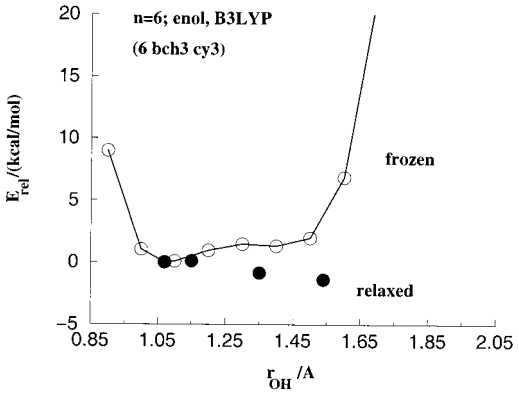

Figure 4. Comparison of the potential energy profile as a function of the *r*(O···H) separation for enol (6 bch3 cy3) at the B3LYP/6-311++G-(d,p) level for frozen (○) and relaxed (●) calculations.

If the entire complex is relaxed in the PT-A conformation, the energy of the zwitterion form drops 1.4 kcal/mol below that of the enol form. Also, the enol → PT-A barrier decreases to about 0.1 kcal/mol. As these calculations are extremely time consuming (several hundred hours per optimized structure), a detailed potential energy curve and reaction path for the proton motion could not be mapped out. However, it is clear that the enol → PT-A proton transfer step is exoergic and that the barrier to proton transfer to form the PT-A zwitterion is low.

C. 7-Hydroxyquinoline: Proton Transfer from the NH Group. Calculations at the SCF Level. The proton transfer from the ring N_1 atom of 7-KQ is more complex, because proton transferred forms were found for both the bifurcated (6 bch3 cy3) and the (6 ch4 ch3 cy3) isomers, shown in Figure 6. In analogy to the calculations on the enol clusters, "frozen" and relaxed N−H···N_C proton translocation scans were performed for the 7-ketoquinoline·$(NH_3)_n$, $n = 2-6$ clusters. The proton transfer potential energy curves along the N−H···N coordinate show two distinct minima (see Figure 5a); the proton transferred minimum is denoted PT-C. The N_1 → N_C forward barrier decreases from ∼50 kcal/mol for $n = 2$ to ∼25 kcal/mol for $n = 6$. Interestingly, the keto → PT-C barrier for (6 ch4 ch3 cy3) is lower than that for (6 bch3 cy3) (see Figure 5a), in contrast to their enol → PT-A barriers (Figure 3a). The N_C → N_1 reverse barrier decreases between $n = 2$ and $n = 3$ and remains at ∼5 kcal/mol for larger *n*. For increasing *n*, the equilibrium $r_e(N_1\cdots H)$ distances in the keto forms remain almost unchanged whereas those of the PT-C minima decrease monotonically with increasing *n*.

Full structure optimization for the (6 ch4 ch3 cy3) isomer and its PT-C form results in a marked decrease of the forward barrier from 25 to 10 kcal/mol (see Figure 5b). The decrease by a factor of 2.5 is comparable to that calculated for the enol → PT-A proton translocation. Structural optimization of the PT-C (6 bch3 cy3) zwitterion invariably converged to (6 ch4 ch3 cy3) for H···N_C distances of >1.6 Å.

The decrease of N···N distance accompanying the N_1 → N_C proton transfer is 0.5 Å (see Figure 5c). This corresponds to a stronger coupling between N_1−H and $N_1\cdots N_C$, as compared to the 0.35 Å change for O−H → N_A transfer in the enol form (see Figure 3c).

Calculations at the B3LYP Level. Inclusion of electron correlation energy at the DFT level leads to important changes: first, the optimized (6 bch3 cy3) and (6 ch4 ch3 cy3) structures of keto 7-HQ·$(NH_3)_6$ were found to differ in total energy by only 0.86 kcal/mol (see Figure 7). Because (6 ch4 ch3 cy3) is lower in energy, a frozen-cluster scan was performed

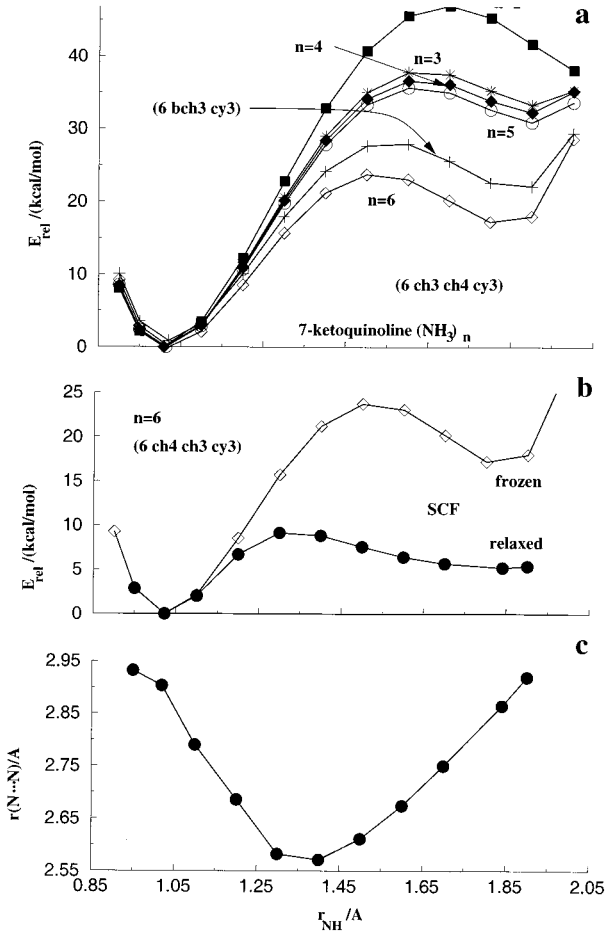

Figure 5. (a) Same as Figure 3 but along the N−H···N proton translocation coordinate in keto 7-HQ·$(NH_3)_n$ ($n \leq 6$). (b) As in Figure 3b but for (6 ch4 ch3 cy3). (c) Separation N···N as a function of the N···H distance.

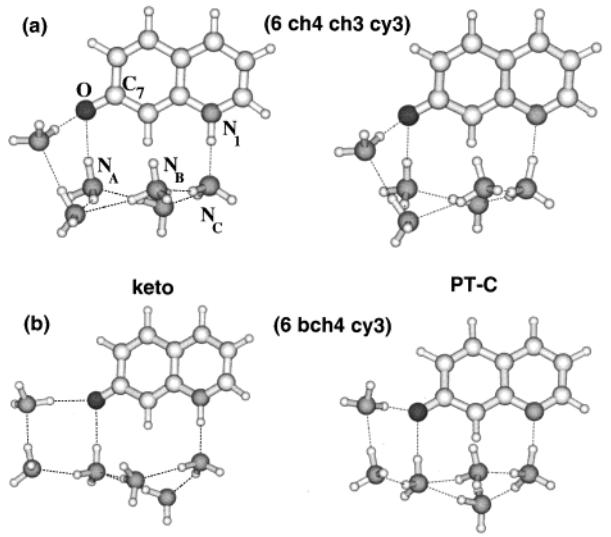

Figure 6. B3LYP/6-311++G(d,p) optimized minimum energy structures of the keto (left) and corresponding PT-C form (right) of 7-HQ·$(NH_3)_6$: (a) (6 ch4 ch3 cy3) isomer; (b) (6 bch3 cy3) isomer. In addition, selected atoms on 7-HQ are numbered as referenced in the text.

along the proton translocation coordinate. The forward barrier is relatively high, ∼8.5 kcal/mol, and leads to a shallow minimum, as shown in Figure 7. Structure optimization of this PT-C form results in a reaction energy of $\Delta_r E = 0.90$ kcal/mol, relative to the keto 7-HQ·$(NH_3)_6$ minimum (see Figure 7). Repeating a structural optimization on PT-C for (6 bch3 cy3) now yields a stable local minimum, 3.3 kcal/mol above the keto energy, in contrast to the situation found for the SCF calculations, see above.

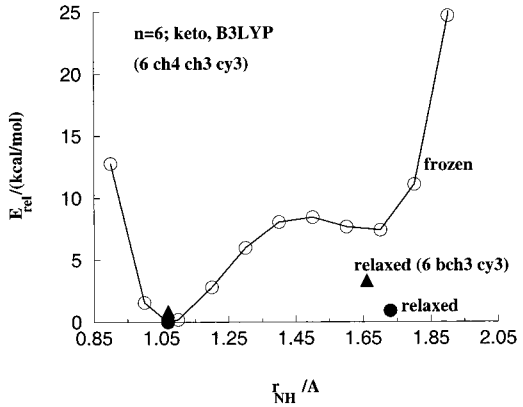

Figure 7. Comparison of the energy profile as a function of the N−H separation for keto (6 ch4 ch3 cy3) at the B3LYP/6-311++G(d,p) level for constrained (○) and relaxed (●) calculations. The Δ symbolizes the keto and PT-C form of (6 bch3 cy3); all energies are relative to the optimized keto (6 ch4 ch3 cy3) structure.

It is instructive to consider the effects of proton transfer on the geometric changes in 7-ketoquinoline while PT takes place. Surprisingly, the calculations predict that the change of N_1-N_C distance is about 0.01 Å. The H-bond becomes nonlinear, as the $N_1\cdots H\cdots N_C$ angle decreases from 177 to 170 °. Larger changes apply to the internuclear distances in the solvent. The bond between N_C and N_B contracts from 3.17 to 2.79 Å. Clearly this change is induced by the charge transfer into the cluster. Also, the hydrogen bonds within the solvent network are not really linear. They form an angle of ∼170°.

The B3LYP/6-311++G(d,p) calculations give the following overall energy profile for 7-HQ·$(NH_3)_6$: the global minimum structure is the PT-A zwitterion. The enol 7-HQ cluster lies 1.4 kcal/mol higher in energy, while on the keto side of the path, the 7-KQ cluster and the PT-C zwitterion correspond to locally stable minima which lie 6.9 and 7.7 kcal/mol higher than PT-A.

Discussion

The experimental results have been described above. Most significantly to the following discussion, it was found that for ammonia cluster sizes $n < 5$ only the enol tautomer is stable. In addition, the spectra suggest that for $n \geq 5$ the zwitterion cluster becomes the globally stable species.

In line with these observations, the present calculations predict the enol tautomer to be the only stable species for ammonia clusters up to $n = 5$. As the cluster size increases to $n = 6$, proton transferred zwitterion structures become *locally* stable at the SCF/6-31G(d,p) level, viz. Figure 3b, and *globally* stable at the B3LYP/6-311++G(d,p) level, where the PT-A zwitterion is calculated to lie 1.4 kcal/mol below the enol cluster, cf. Figure 4. At the other side of the proton transfer path, both the (6 ch4 ch3 cy3) and (6 bch3 cy3) forms of the keto tautomer and the PT-C zwitterion lie above the globally stable PT-A zwitterion by 6.9 and 7.7 kcal/mol, respectively. This implies that the keto tautomer is *not* formed in the electronic ground state for the $n = 6$ cluster.

Having established the existence of local minima PT-A and PT-C for $n = 6$, further transport of the proton along the ammonia wire was investigated. Starting from the PT-A minimum, the most obvious reaction path involves displacing

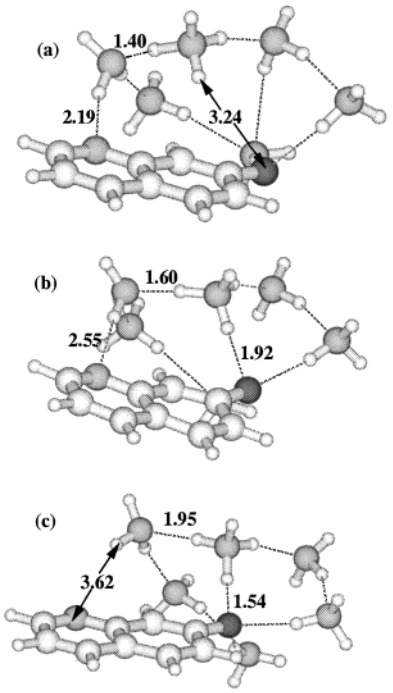

Figure 8. A series of optimized PT-B′ cluster structures, illustrating the large-scale diffusive motion accompanying proton transfer: (a) for $r(N_C\cdots N_B)$ constrained at 1.40 Å; (b) for $r(N_C\cdots N_B)$ constrained at 1.60 Å; (c) fully optimized structure, resulting in $r(N_C\cdots N_B) = 1.95$ Å. Note the motion of the entire cluster relative to the 7-hydroxyquinoline framework, as well as large individual variations of N···N distances and relative orientation angles. All calculations at the SCF/6-31G(d,p) level.

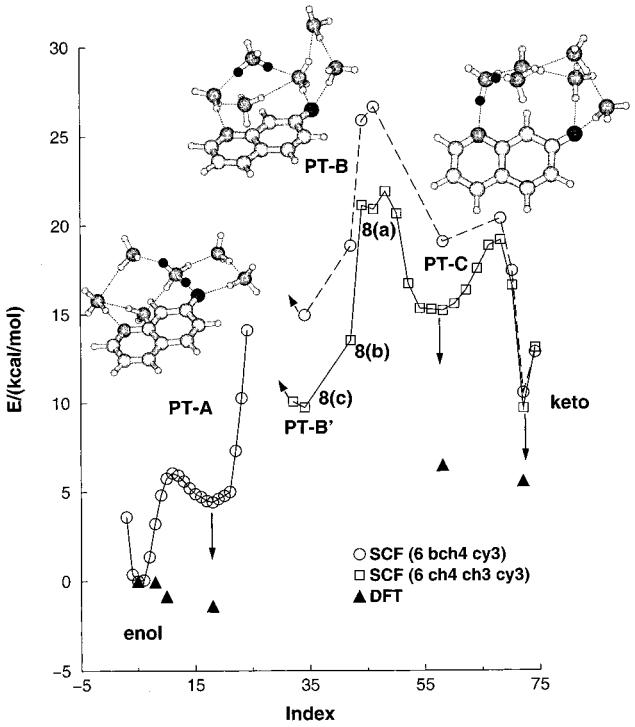

Figure 9. Calculated energy profiles for some major proton transfer reaction paths in the 7-HQ·$(NH_3)_6$ cluster. The index indicates the progression along the four local proton transfer driving coordinates: Starting from the enol tautomer at left, the coordinate changes at the PT-A, PT-B or PT-B′, and PT-C zwitterionic minima; see text. All energies are given relative to the enol (6 bch3 cy3) cluster. In the inserted zwitterion structures PT-A, PT-B, and PT-C, the "coming" and "going" protons are marked in black. The proton transfer coordinate is constrained and typically advances in steps of 0.05 Å along the respective O···H or N_i···H distance; all other coordinates are optimized. Open symbols refer to SCF/6-31G(d,p) calculations: ○ symbolizes the (6 bch4 cy3) isomer and □ the (6 ch4 ch3 cy3) structures. Filled triangles indicate B3LYP/6-311++G(d,p) optimized structures. Solid lines with arrows connect SCF/6-31G(d,p) minima with their B3LYP/6-311++G(d,p) analogues. Labels 8(a), 8(b), 8(c) refer to the structures shown in Figure 8.

the proton toward ammonia molecule B along the $N_A\cdots N_B$ internuclear axis. However, this path turned sharply upward and eventually leads to partial disruption of the hydrogen bond network of the cluster. The alternative proton transfer path along the lower branch of the bifurcated chain is symmetry-equivalent to the upper.

Exploring the reverse path, displacing the proton from the keto (6 ch4 ch3 cy3) isomer via the PT-C zwitterion and further along the chain toward NH_3(B) leads to another locally stable zwitterion denoted PT-B′ (see Figure 8). Displacing the proton along the $N_C\cdots N_B$ internuclear axis and performing constrained optimizations gives structures displayed in Figure 8. In Figure 8a and b, $r(N_C\cdots H)$ was constrained at 1.40 and 1.60 Å, respectively. The final structure PT-B′ in Figure 8c follows by full optimization, resulting in $r(N_C\cdots H) = 1.95$ Å. Comparing the cluster structures shown in Figure 8 shows that the shift of the proton from NH_3 molecule C to B is accompanied by large-scale translational motions of the entire cluster relative to the 7-HQ framework. These results are combined with the PT path between keto (6 ch4 ch3 cy3) and its PT-C form (shown in Figure 5) and displayed on the right-hand side in Figure 9.

A different reverse path, starting from the (6 bch3 cy3) isomer of PT-C was also explored because a *direct* path between enol and keto 7-HQ·$(NH_3)_6$ seemed possible. Several constrained SCF/6-31G(d,p) calculations between keto 7-HQ·$(NH_3)_6$ and PT-C isomerized to the (6 ch4 ch3 cy3) isomer. The structure around PT-C is a constrained optimization and does not lead to a locally stable PT-C (6 bch3 cy3) isomer if the N_C-H distance is optimized. A constrained scan lead over a barrier of 8.50 kcal/mol into a shallow minimum to the zwitterion isomer denoted PT-B. This structure is only marginally stable with respect to further translocation of the proton toward PT-A. Stretching the N_B-H distance leads to a reorganization of the cluster H-bond network. This potential energy profile is also shown in Figure 9, with the PT-A and PT-B structures shown as insets.

Figure 9 collects the main findings of our computational investigations of proton transfer in 7-HQ·$(NH_3)_6$. The open points refer to r(O···H)- or r(N···H)-constrained but otherwise structure-optimized SCF/6-31G(d,p) calculations. A reaction path index sequentially orders the optimized structures and energies obtained along any given proton translocation coordinate. Note that, at each minimum, the translocation coordinate changes. Thus, starting from the enol tautomer on the left, the translocation of the proton from the O−H group toward PT-A is followed, leading over a 6.1 kcal/mol barrier to a first local minimum, 4.4 kcal/mol higher. From index point 18 to the right, the A → B translocation path is followed, displacing the proton toward molecule B, which leads steeply uphill. Starting from the keto tautomer (6 ch4 ch3 cy3) on the right-hand side of Figure 9 (reaction path index 72), the path leads over a first barrier at index point 68 to the PT-C zwitterion at #58, and across another higher barrier at 50 to the PT-B′ minimum 9.9 kcal/mol above the enol tautomer. The alternative path from the (6 bch4 cy3) isomer to PT-C and PT-B is indicated with squares.

We were not able to find a contiguous proton transfer reaction path leading from either PT-A toward PT-B or PT-B′ or in the reverse direction. In this region of the reaction path, large-scale structural reorganizations of the cluster occur, which lead across high barriers and cannot be easily followed with the present approach, since they always result in structural instabilities of the cluster. The barriers are high enough to render the region indicated by dashed lines around PT-B the bottleneck for proton transfer along the ammonia chain.

The insets in Figure 9 show that the initial (enol ↔ PT-A zwitterion) and final (PT-C ↔ keto) proton transfer steps are Grotthus-type or hopping proton transfers: they involve a proton hop directly along the O−H···N or N−H···N hydrogen bond. The proton motion is coupled to a transient decrease of the intermolecular O···N or N···N stretching coordinate. In the following PT-C ↔ PT-B or PT-C ↔ PT-B′ steps, a *different* proton leaves the NH_4^+ ion, which amounts to the Grotthus proton transfer model.

In contrast, along the reaction path that leads from PT-B′ toward the enol tautomer, proton hopping seems *not* to be strongly involved. The proton motion from the NH_3(B) molecule toward the O^- atom is coupled to a diffusive-type large-scale motion of the entire solvent cluster, very different from a Grotthus-type proton translocation. Similar observations apply to the reaction path that leads from PT-B towards the enol tautomer. In both cases, there is no proton hopping. Charge migration involves diffusion, hydrogen bond rearrangement, or both and the reaction path is long and contorted.

Figure 9 also shows that the stability of the different zwitterion forms PT-A, PT-B, PT-B′, and PT-C is qualitatively correlated with the *number of hydrogen bonds* formed by the NH_4^+ ion. In the most stable zwitterion PT-A, the NH_4^+ forms four hydrogen bonds, in the PT-C zwitterion, only three hydrogen bonds, at an energetic cost of about 10 kcal/mol. The PT-B zwitterion with only two hydrogen bonds lies another 10 kcal/mol higher. The PT-B′ zwitterion (Figure 8c) forms three hydrogen bonds and lies between PT-A and PT-C. This implies that proton transfer along an isolated chain of NH_3 molecules in which the NH_4^+ ion can only form two hydrogen bonds at a time is a high-barrier process. Low-barrier proton transfer within the cluster occurs only toward NH_3 molecules that have *at least local 3- or 4-fold hydrogen bond coordination*. In other words, the local "polarization well"[1] accompanying the moving proton dictates that the next hop can only occur to a locally 3- or 4-fold-coordinated NH_3 molecule; if no such molecule exists, as for PT-A, the proton is blocked from further hops.

The importance of local 4-fold hydrogen bond coordination is also seen in the $n = 5$ cluster: there, in all calculations thus far carried out at the SCF and B3LYP levels, proton transfer from the enol OH to the closest ammonia does not result in a stable minimum for the PT-A structure. We believe that this is because the A-ammonia molecule is only 3- and not 4-fold coordinated. The sixth ammonia molecule provides full 4-fold coordination of this molecule, leading to better solvation of the NH_4^+ ion.

In the cluster size range $n = 4-10$ discussed here, the solvation of 7HQ is still far from complete. These relatively small solvent clusters do not provide the stabilizing inductive and dispersive long-range contributions that occur in bulk solutions or biological environment. Therefore, correlations to macroscopic solution spectra are necessarily limited. However, the important point is that the experimental results (see Figure 1) show that the large changes in the spectra of the systems happen between $n = 3$ and $n = 6$, while between $n = 6$ and $n = 10$, the spectral changes are relatively minor. As shown above, they can be correlated with the occurrence of characteristically different exothermic proton transfer steps by the calculations.

Conclusions

Supersonic jet-cooled 7-HQ·$(NH_3)_n$ ($n \leq 10$) clusters were investigated by means of 2C-R2PI spectroscopy. With increasing cluster size, the spectral features change considerably: up to $n = 4$, the R2PI spectra are characteristic of clusters containing the neutral enol tautomer. A broad band indicating the 7-HQ^- anion appears at $n = 5$ or 6, implying that the threshold to ground-state proton transfer and concurrent formation of zwitterion clusters is at $n = 5$ or 6. Absorption bands characteristic of the 7-ketoquinoline tautomer appear at $n > 6$.

Extended ab initio calculations of the proton transfer reaction paths up to $n = 6$, starting from both the enol and keto tautomers, show gradual stabilization of proton transferred forms as n increases. Locally stable zwitterion 7-HQ^-·$H^+(NH_3)_n$ structures appear for $n = 6$ at the SCF level. Full structural optimizations at the B3LYP/6-311++G(d,p) level lead to the conclusion that 7-HQ·$(NH_3)_6$ is the smallest cluster to show a globally stable zwitterion form, denoted PT-A. This implies exoergic enol → PT-A ground-state proton transfer for $n = 6$ in the cold cluster, which is in qualitative agreement with the 2C-R2PI spectra.

Starting from the enol tautomer, the first, third, and fourth proton transfer steps along the ammonia cluster in 7-HQ·$(NH_3)_n$ are Grotthus-type proton hops along an "ammonia wire", in which 3- and 4-fold hydrogen-bonded NH_3 molecules are involved. We find a qualitative correlation between the hydrogen bond coordination number of the NH_3 acceptor molecule and the stability of the zwitterion cluster.

In the region between the PT-A and PT-B (or PT-B′) zwitterion structures, where the proton has to pass along a 2-fold hydrogen-bonded NH_3 molecule, the proton motion is very different from a hopping mechanism. Proton transfer is accompanied by large structural changes of the cluster involving single-molecule rototranslational as well as collective diffusive motions. It is particularly this region that needs further investigation and attention.

We stress that the calculations and discussion presented above reflect only a static view. The influences of temperature, vibrational excitation, and quantum effects are not yet taken into account. To do so would necessitate calculations of large portions of the high dimensional potential energy surface, a computational task that exceeds our current possibilities but might be feasible in the future.

Acknowledgment. The authors acknowledge financial support from the Schweiz. Nationalfonds (project no. 20-53932.98) and computer time provided by the Centro Svizzero di Calcolo Scientifico (CSCS) in Manno, Switzerland.

JA010893A